Inertia–Gravity Wave Breaking in Three Dimensions. Part II: Convectively Unstable Waves

M.-PASCALE LELONG AND TIMOTHY J. DUNKERTON

Northwest Research Associates, Bellevue, Washington

(Manuscript received 29 January 1997, in final form 24 September 1997)

ABSTRACT

The three-dimensional breakdown of a large-amplitude, convectively unstable inertia–gravity wave is examined numerically as a function of primary-wave frequency and amplitude. The results confirm that near-inertial waves break down preferentially via shear instability even when the primary wave is initially overturned. As in the convectively stable near-inertial regime, the spectrum of instability energy is approximately isotropic in azimuthal orientation. At intermediate frequencies, wave breakdown is triggered by a transverse shear instability in the region of overturning. This behavior, displaying a clear preference for instability with horizontal component of wavevector in the transverse direction, is different from the breakdown of convectively stable waves at intermediate frequency examined in Part I. As the primary-wave frequency is increased further, shear instabilities once again develop in the transverse direction, but they are modified by convective instability as the billows reach finite amplitude. The influence of transverse vertical shear becomes progressively weaker as the wave frequency approaches the buoyancy frequency. In this limit, transverse convection leads to wave collapse, and there is no preferred scale of instability.

1. Introduction

In a companion paper (Lelong and Dunkerton 1998, hereafter LD1), we used a three-dimensional nonlinear numerical model to examine the onset of instability in large-amplitude, convectively stable inertia–gravity waves (IGWs) in the parameter range $0.6 \leq R \leq 0.95$, where $R \equiv f/\omega$; f and ω denote the Coriolis and primary-wave frequencies, respectively. In this region of parameter space, LD1 found that IGW are unstable to shear instability. For low-frequency, near-inertial waves ($0.9 \leq R \leq 0.95$), instabilities develop nearly simultaneously in all azimuths and at most phases of the wave. The spectrum of instability energy is therefore approximately isotropic in azimuthal orientation. By contrast, for intermediate-frequency waves in the range $0.6 \leq R \leq 0.8$, the instability is confined near the region of reduced static stability and is oriented primarily at intermediate azimuths (e.g., near 45°). Near-inertial waves exhibit the fastest growing instabilities, with growth rates dropping off rapidly below $R \leq 0.9$. At all but the lowest frequencies investigated, the threshold amplitude for modal shear instability is located somewhat above the theoretical stability boundary $a_s = a_s(R)$ determined from a local Richardson number argument (Dunkerton 1984; Fritts and Rastogi 1985).

In this paper, we examine what happens when the primary wave is initially overturned or convectively unstable. In the notation of LD1, this regime corresponds to the region of parameter space with $a > 1$, where a is a nondimensional measure of wave amplitude such that $a = 1$ in convectively neutral waves. A linear stability analysis was performed by Dunkerton (1997), who suggested that the convectively unstable regime can be divided roughly into three regions depending on the value of R (i.e., depending on the importance of rotation):

1) For low-frequency waves near the inertial cutoff ($R \rightarrow 1$), shear instability is the dominant mode of breakdown at all amplitudes above a_s, convectively stable or unstable, and is approximately isotropic in azimuthal orientation.
2) For intermediate-frequency waves ($0.4 \lesssim R \lesssim 0.7$), the dominant mode at lower horizontal wavenumbers is a transverse shear instability (or hybrid shear/convective instability).
3) For high-frequency waves ($R \rightarrow 0$), transverse convection prevails, and there is a slower-growing mode of parallel shear instability in the zonal direction as observed in the nonrotating case (e.g., Dunkerton and Robins 1992).

The analysis of Dunkerton (1997) was based on a steady, parallel-flow approximation to IGW motion. While this

Corresponding author address: Dr. Timothy J. Dunkerton, Northwest Research Associates, Inc., P.O. Box 3027, Bellevue, WA 98009-3027.
E-mail: tim@nwra.com

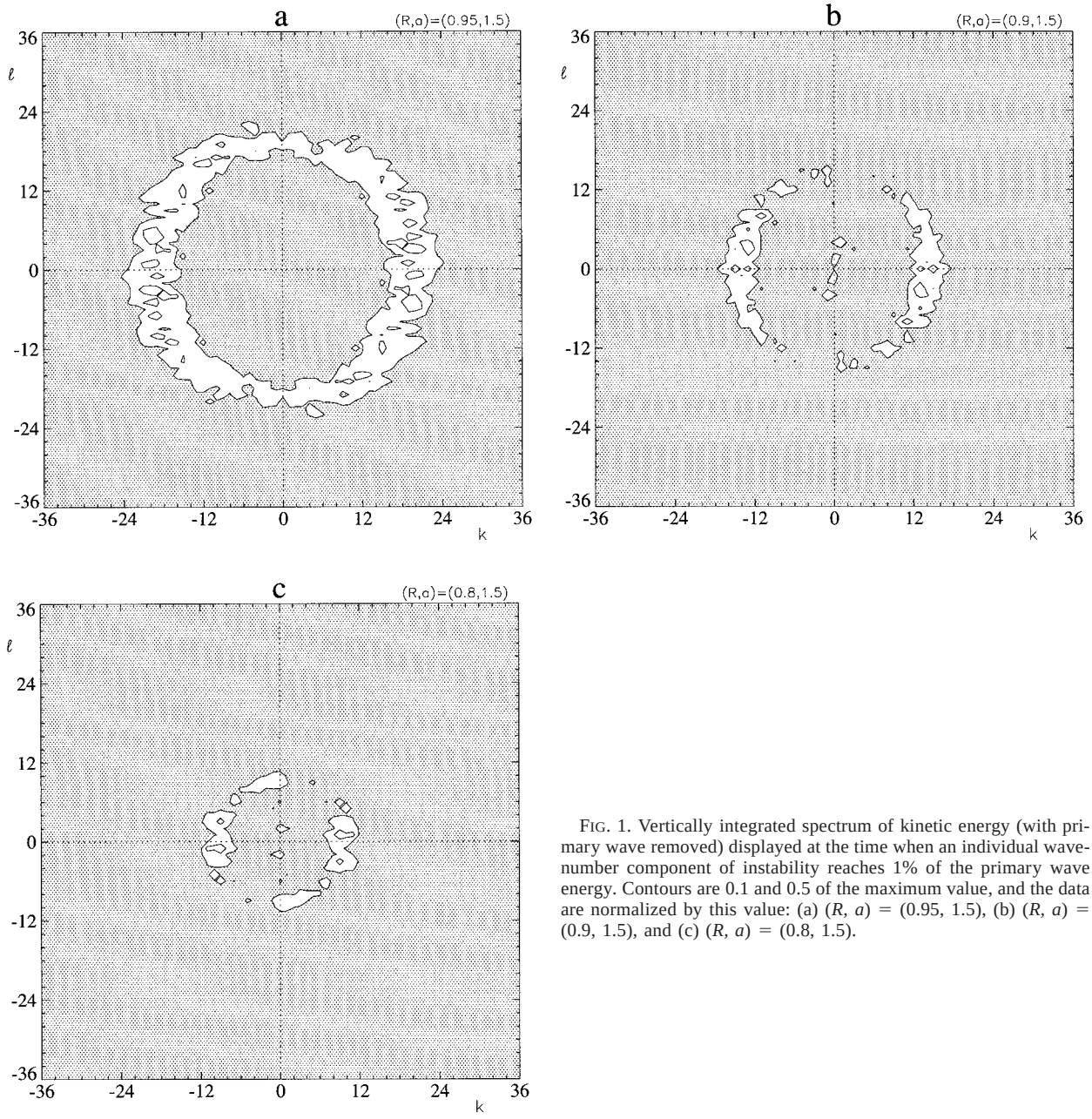

FIG. 1. Vertically integrated spectrum of kinetic energy (with primary wave removed) displayed at the time when an individual wavenumber component of instability reaches 1% of the primary wave energy. Contours are 0.1 and 0.5 of the maximum value, and the data are normalized by this value: (a) (R, a) = (0.95, 1.5), (b) (R, a) = (0.9, 1.5), and (c) (R, a) = (0.8, 1.5).

approximation is expected to become more accurate as wave amplitude is increased, because growth rates increase, it is desirable to confirm Dunkerton's predictions, and—going beyond a linear stability analysis—to investigate the finite-amplitude behavior of IGW instabilities and their ability to saturate the primary wave. In LD1, the problem of IGW breakdown was posed for convectively stable waves. It is worthwhile to investigate this case because, in any real situation involving growing waves, IGWs become susceptible to shear instability prior to the onset of convective overturning. Our results in this region of parameter space agreed with Dunkerton's (1997) analysis at large R, but revealed some unexpected behavior at intermediate R.

The convectively unstable regime is well above the theoretical stability boundary at intermediate and large R, and may therefore seem irrelevant. It should be noted, however, that this region of parameter space is accessible whenever the central amplitude of an inertia–gravity wave packet grows sufficiently fast (e.g., due to critical-layer approach or ambient density decreasing with height) so that weakly growing shear instabilities adjacent to the stability boundary do not have time to develop. Moreover, for intermediate- and high-

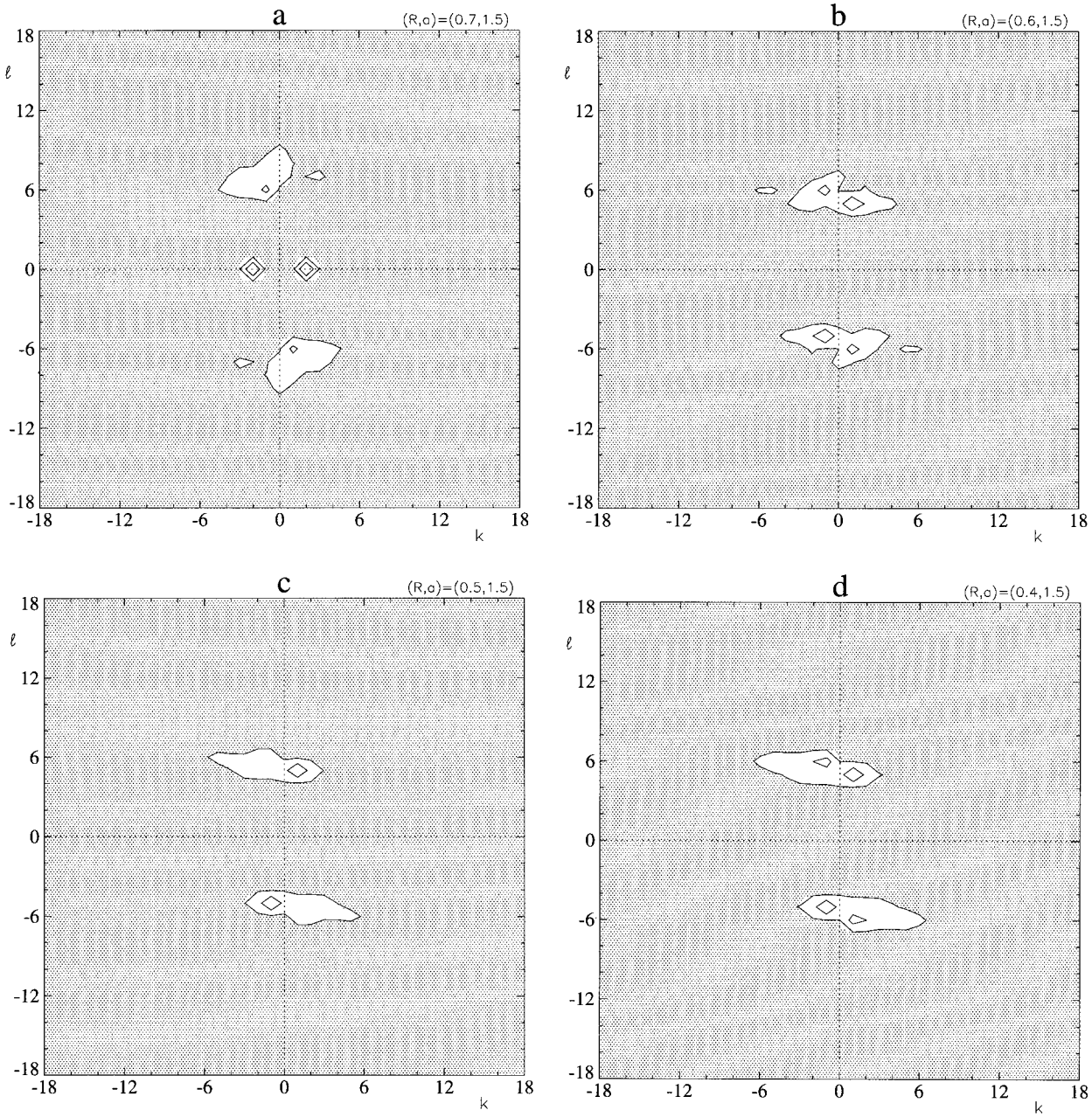

FIG. 2. Vertically integrated kinetic energy spectrum as in Fig. 1 but for (a) (R, a) = (0.7, 1.5), (b) (R, a) = (0.6, 1.5), (c) (R, a) = (0.5, 1.5), and (d) (R, a) = (0.4, 1.5).

frequency waves ($R \lesssim 0.5$) the regime $a < 1$ is, for practical purposes, stable with respect to local shear instabilities (Fritts and Yuan 1989; Dunkerton 1997; LD1). Whether a certain type of instability is realized in any given situation depends, among other things, on the vertical group velocity of IGW, shape of IGW packet, and initial noise level. This is a complicated problem that we have simplified, as in LD1, by assuming a monochromatic, triply periodic IGW motion with constant wave amplitude prior to breakdown. In general, an IGW packet can be expected to propagate vertically (as a group) some fraction of its characteristic vertical wavelength within one intrinsic wave period. This fraction approaches zero as $R \rightarrow 1$ (approaching a critical level) but is significant for intermediate R. Thus (for instance) in a quasi-compressible atmosphere at rest, a significant increase of wave amplitude may occur at the leading edge of the wave packet within a few wave periods, whereas (for simplicity) we assume a constant amplitude, as might be found in an equili-

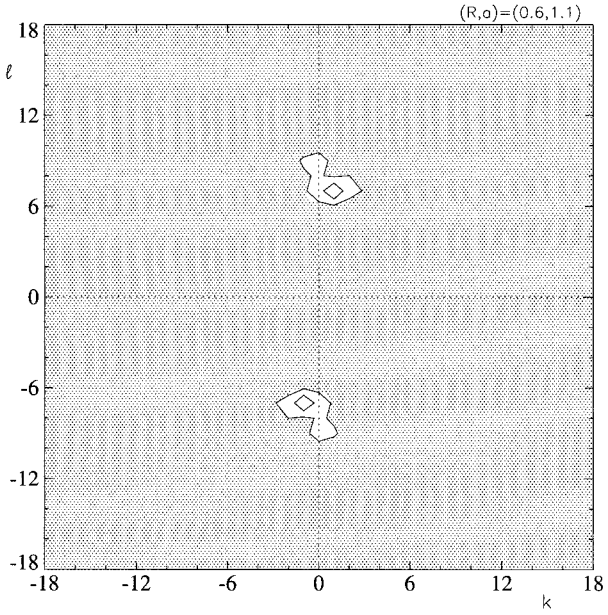

FIG. 3. Vertically integrated kinetic energy spectrum as in Fig. 1 but for $(R, a) = (0.6, 1.1)$.

brated wave packet maintained by constant lower-boundary forcing.

Early numerical studies of internal wave propagation and breakdown focused on nonrotating, high-frequency waves in a two-dimensional domain restricted to the vertical plane of propagation (Winters and D'Asaro 1989; Walterscheid and Schubert 1990; Dunkerton and Robins 1992). The 2D simulations demonstrated that convectively unstable waves break down via local shear or convective instability (or some combination of the two) depending on the circumstances, in agreement with a linear stability analysis confined to the plane of wave propagation (e.g., Dunkerton and Robins 1992). However, the stability analysis of Winters and Riley (1992)[1] and subsequent three-dimensional numerical simulations illustrated the importance of allowing for fluid motion in a direction transverse to the plane of propagation (Winters and D'Asaro 1994; Andreassen et al. 1994; Fritts et al. 1994; Isler et al. 1994; Lombard and Riley 1996). When the third dimension is taken into account, the dominant instability consists of counter-rotating vortices with axes oriented parallel to the direction of wave propagation and confined to the region of convective overturning. In this case, the horizontal component of instability wave vector points in the transverse direction; therefore we refer to such instabilities as "transverse" convection. When the third dimension is suppressed, transverse convection cannot take place, and the flow exhibits unrealistically long-lived regions of overturned fluid due to the fact that parallel shear and convective instabilities take longer to develop (Dunkerton 1997).

Rotation alters the structure of internal gravity waves and introduces a new feature, namely, a component of vertical shear in the transverse direction, associated with the transverse velocity component of IGWs due to the Coriolis force. The parallel and transverse components of horizontal velocity are in quadrature, with transverse vertical shear maximizing at the extrema of local static stability. [The latter combination, for sufficiently large but convectively stable wave amplitude, allows the possibility of a local Richardson number below 1/4 (Dunkerton 1984; Fritts and Rastogi 1985). This requirement for shear instability is trivially satisfied in convectively unstable waves.] Shear, as is now well understood, tends to counteract the destabilizing effects of convection in the plane of the shear but does not influence motions outside of this plane (Deardorff 1965; Winters and Riley 1992). It is for this reason that transverse convection grows more rapidly than parallel convection in the convectively unstable nonrotating case discussed above. We will show that the nature of instability in convectively unstable IGW depends on the relative strength of vertical shear in the plane transverse to the wave propagation, hence, on the value of R.

The paper is organized as follows. A brief description of the numerical model is given in section 2 (the reader is referred to LD1 for more details of the numerical method). Results are presented in section 3. We identify three distinct regimes of instability as the primary-wave frequency is varied. The behavior of instability changes from shear driven and approximately isotropic at the lowest frequencies (section 3a), to shear driven but confined primarily to the transverse direction at intermediate frequencies (section 3b), to a hybrid shear–convective regime where shear may or may not influence scale selection but cannot, in any case, prevent the outbreak of convection (section 3c). A summary of growth rates as a function of R and a is given in section 3d. Conclusions and a brief discussion of items for future research are included in section 4.

2. Numerical model

As described in LD1, our pseudospectral numerical model solves the three-dimensional Boussinesq equations of momentum and a density equation in a triply periodic domain. The initial condition consists of randomly phased white noise superposed on a single, downward phase-propagating linear inertia–gravity wave with wavenumber $(k, l, m) = (k_{\min}, 0, m_{\min})$ in a computational domain of width $L_x = L_y = 2\pi/k_{\min}$ and height $L_z = 2\pi/m_{\min}$. The inertia–gravity wave satisfies the polarization relations

[1] Winters and Riley (1992) investigated a family of profiles, with static stability varying twice as rapidly in the vertical as the horizontal velocity, for which analytic solutions can be obtained in the neutral limit (Hazel 1972). Their basic state was two-dimensional and rotation was excluded.

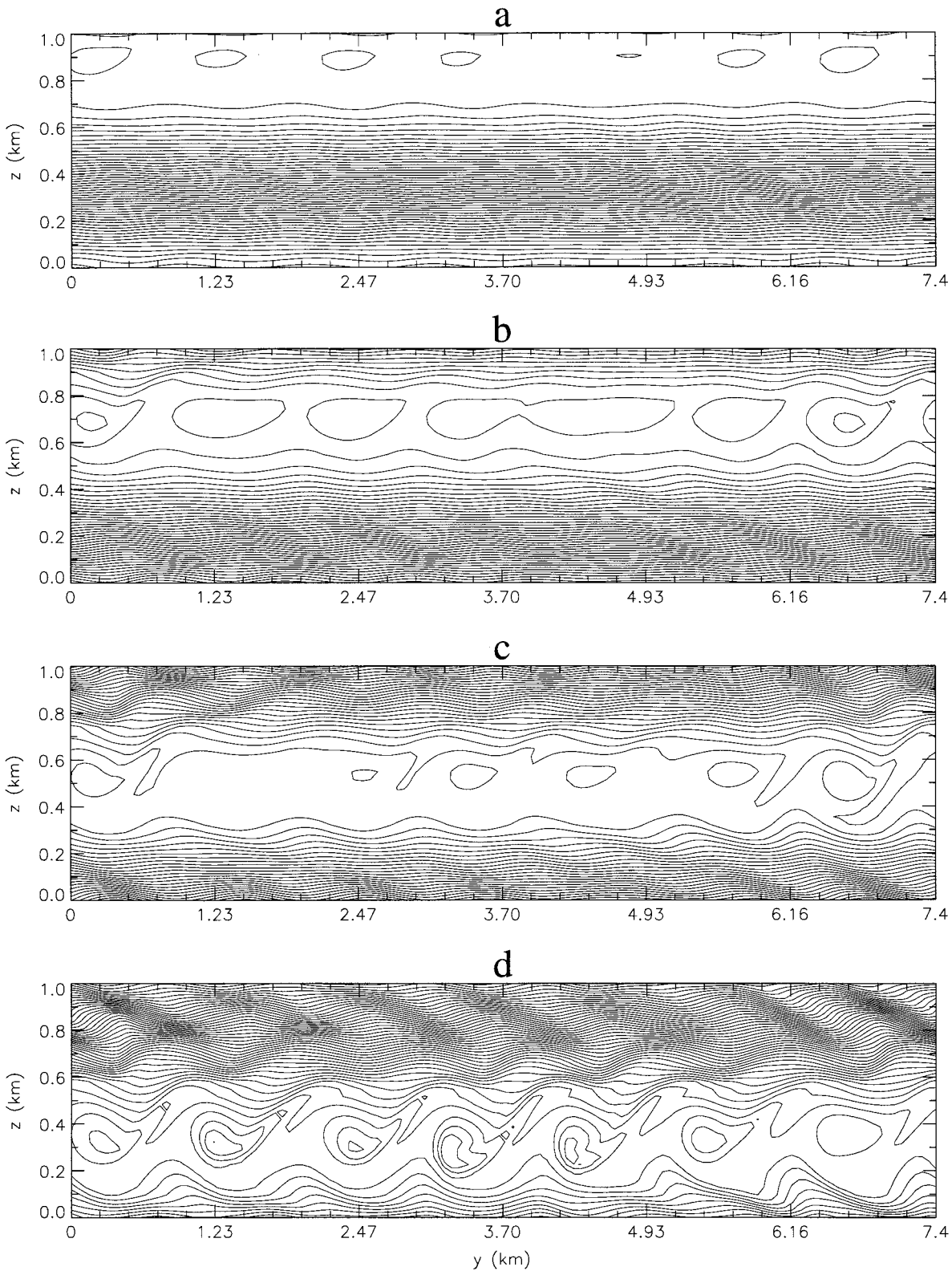

FIG. 4. Time evolution of the density field in a numerical simulation with IGW parameters $(R, a) = (0.6, 1.1)$, displaying the y–z plane at $x = 1.45$ km. Four times are shown, at (a) $t = 2.5T_w$, (b) $t = 2.76T_w$, (c) $t = 2.83T_w$, and (d) $t = 3.0T_w$, where T_w is the IGW period.

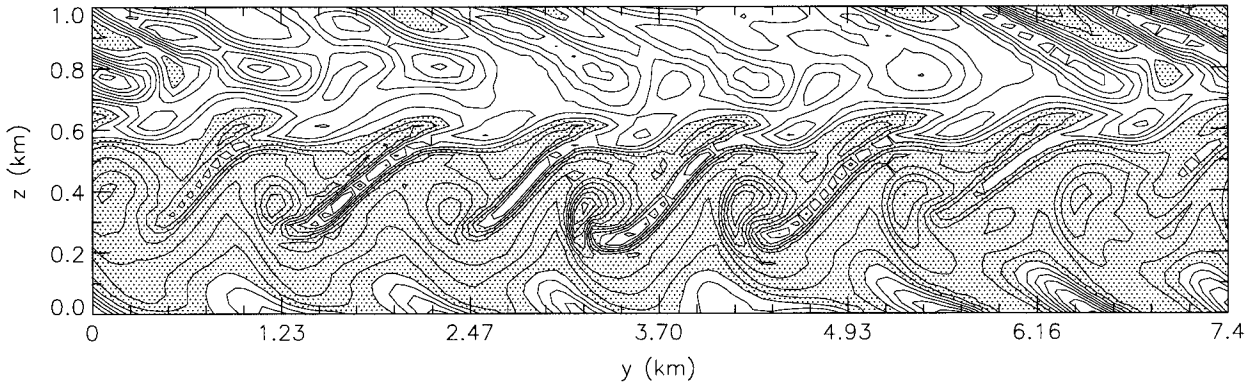

FIG. 5. Parallel vorticity component corresponding to Fig. 4d.

$$u = a\hat{c}\cos\phi, \tag{2.1a}$$

$$v = a\hat{c}R\sin\phi, \tag{2.1b}$$

$$w = -\frac{a\hat{c}k}{m}\cos\phi, \tag{2.1c}$$

$$\frac{g\rho}{\rho_0} = -\frac{aN^2}{m}\sin\phi. \tag{2.1d}$$

The coordinate system is oriented such that wave propagation is in the x–z plane. Wave amplitude has been normalized by ω/k, the intrinsic horizontal phase speed of the wave, and is expressed in terms of the nondimensional parameter a. In all cases discussed here, $a \geq 1$, so that the primary wave is initially overturned. As in LD1, we perform simulations with a reduced value of the parameter N/f in order to maximize the range of resolvable spatial scales. The parameter regime investigated spans $0.2 \leq R \leq 0.95$. The ''parallel'' (x) direction refers to the direction of primary wave propagation, and the ''transverse'' (y) direction indicates the horizontal dimension perpendicular to the propagation.

As instabilities reach finite amplitude and become unstable themselves, the natural tendency of the flow is to cascade energy isotropically to smaller and smaller scales. For $R \leq 0.3$, equal numbers of grid points ($128 \times 128 \times 128$) are needed in x, y, and z during the later stages of the simulations in order to achieve isotropy. For larger values of R ($R \geq 0.4$), isotropy can be attained adequately with $128 \times 128 \times 32$ grid points, due to the longer horizontal scale of IGW in this limit. As in LD1, the vertical wavelength of the primary wave was fixed at $L_z = 1$ km for all parameter combinations and L_x varied to produce the desired IGW frequency ω. The static stability is $N = 2 \times 10^{-2}\ \mathrm{s}^{-1}$ and Coriolis parameter $f = 2 \times 10^{-3}\ \mathrm{s}^{-1}$, so that $N/f = 10$.

3. Results

Three distinct regimes of instability have been identified and are discussed below. In some instances, the locus of most unstable modes evolves in time. Thus, disturbances reaching finite amplitude first are not necessarily the ones that exhibited the fastest initial growth rate. The behavior at early times may also be influenced by the growth of nonmodal structures in a continuous spectrum. In this study, our focus is primarily on modal instabilities. Such ''modes'' represent asymptotic solutions to the linearized governing equations in the limit of infinite time, a situation that can be approximated in a nonlinear numerical model by making the amplitude

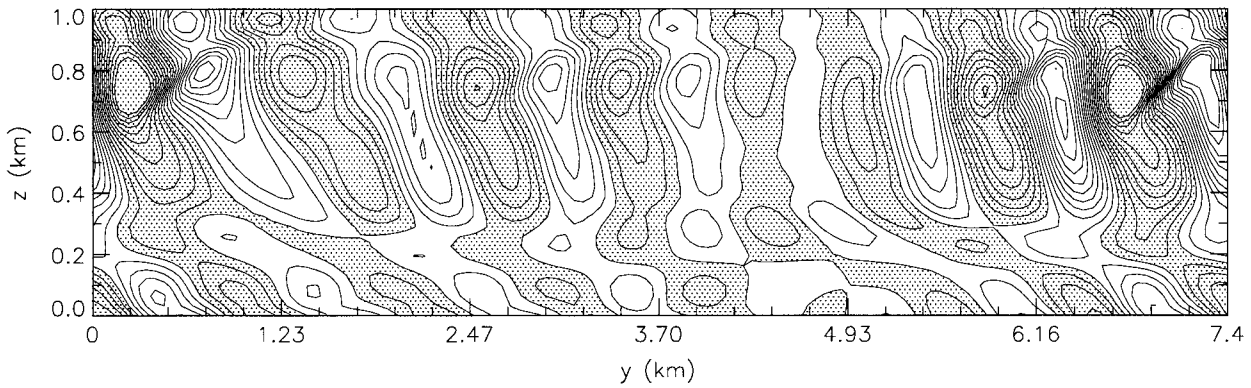

FIG. 6. Perturbation vertical velocity corresponding to Fig. 4b.

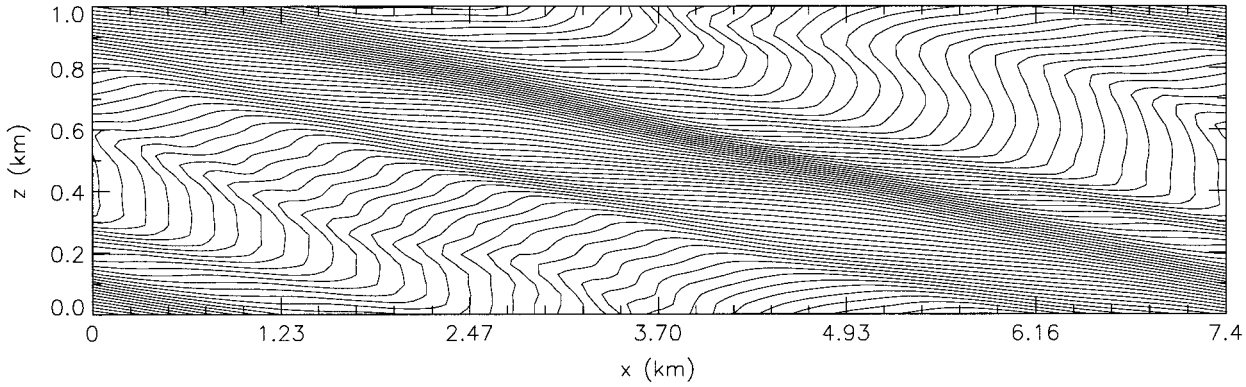

FIG. 7. Vertical cross section of density field in the x–z plane, for IGW parameters $(R, a) = (0.6, 1.1)$, displaying the x–z plane at $y = 4.63$ km.

of initial noise very small (in this case, 10^{-8} relative to the primary IGW). The spectra shown in this section represent approximately the asymptotic state reached before complete nonlinear breakdown of the primary wave. These spectra correspond to the time when the vertically integrated energy at a certain wavenumber (k, l) has grown to 1% of the primary wave's energy. In all cases displayed, the spectra were normalized by the energy in this most energetic wavenumber, and the primary wave masked out.

a. Low-frequency regime: 0.8 < R < 0.95

Figure 1a illustrates the distribution of unstable modes at $R = 0.95$, $a = 1.5$. The ''halo'' structure characteristic of the low-frequency, convectively stable case discussed in LD1 persists at larger, convectively unstable, amplitudes $a > 1$. Aside from an increase in growth rate, the behavior of shear instability at large R does not change as the convective threshold is exceeded. In this case, the growth of shear instability is fast compared to that of convection, which is suppressed by the shear. As noted by Dunkerton (1997), there is a curve $R = R_c(a)$, such that, for $R > R_c$, the growth rate of shear instability is greater than the maximum parcel growth rate of convection (disregarding the effect of shear, which would be to further diminish the importance of convection). It is interesting also to note that in the limit $R \to 1$, the static stability term in the nondimensional Taylor–Goldstein equation becomes insignificant, so that instabilities approach those of unstratified shear flow (Fritts and Yuan 1989). In many respects, then, it seems that shear instability should be the dominant mechanism of breakdown in convectively unstable, as well as stable, IGWs as $R \to 1$. Our numerical results confirm this expectation.

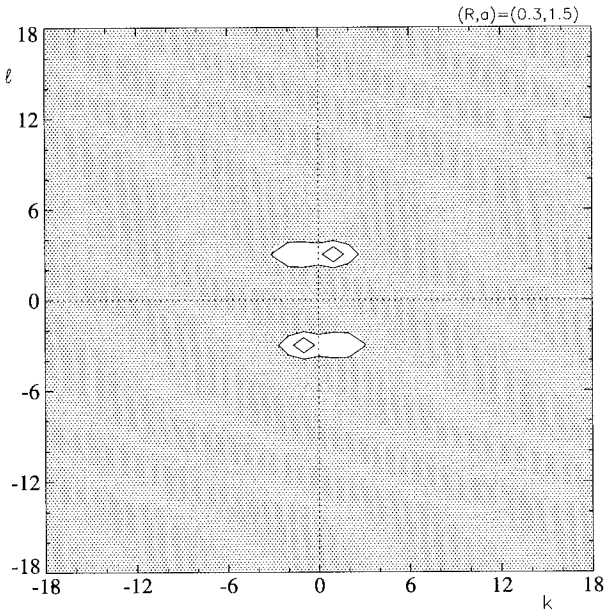

FIG. 8. Vertically integrated kinetic energy spectrum as in Fig. 1 but for $(R, a) = (0.3, 1.5)$.

The isotropic nature of the shear instability persists at $R = 0.9$ (Fig. 1b) and $R = 0.8$ (Fig. 1c) although, at this value of R, the halo is beginning to break up. There is clearly a preference for wavenumbers near 0° azimuth at $R = 0.9$ and 0.8, while in the latter case we also see transverse instabilities beginning to re-emerge. Anisotropy does not necessarily indicate an absence of energy in places where the halo does not connect; rather, that in such places the growth of instability energy has fallen behind the visible parts of the halo (recall that the plots have been normalized by the value at a certain wavenumber having the largest energy at this time). We also note, incidentally, a tendency in these runs for the halo to break up as time progresses, and for the same reason—namely, that certain parts of the halo are slightly more unstable than others. Temporal development of the spectrum is an interesting subject in its own right but will be discussed in another paper in this series.

The contraction of halo radius with decreasing R in Figs. 1a–c is consistent with theoretical expectations. In

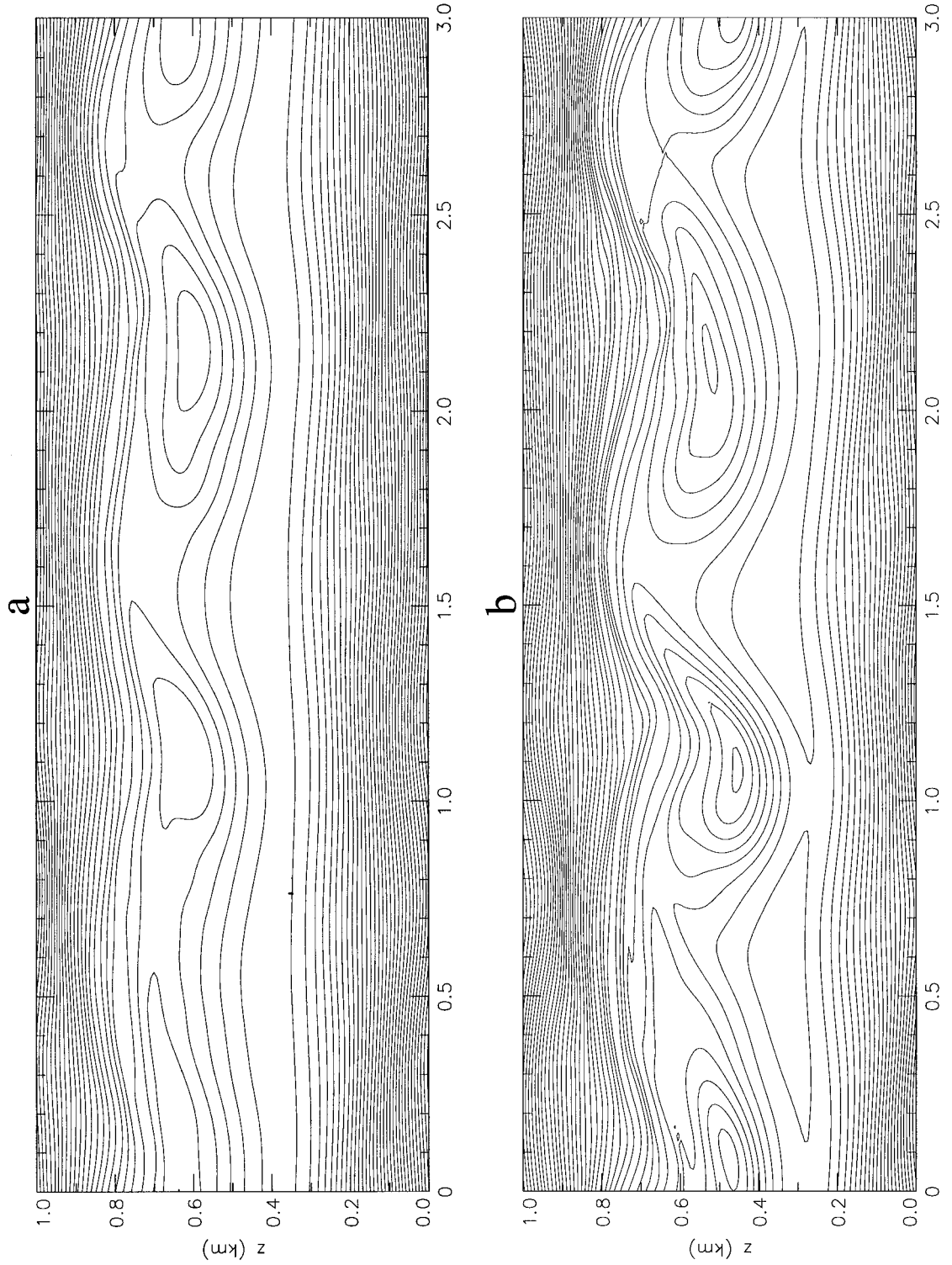

FIG. 9. Time evolution of the density field as in Fig. 4 but for $(R, a) = (0.3, 1.5)$, displaying the y–z plane at $x = 1.16$ km. Four times are shown: (a) $t = 3.58T_w$, (b) $t = 3.67T_w$, (c) $t = 3.83T_w$, and (d) $t = 4.04T_w$, where T_w is the IGW period.

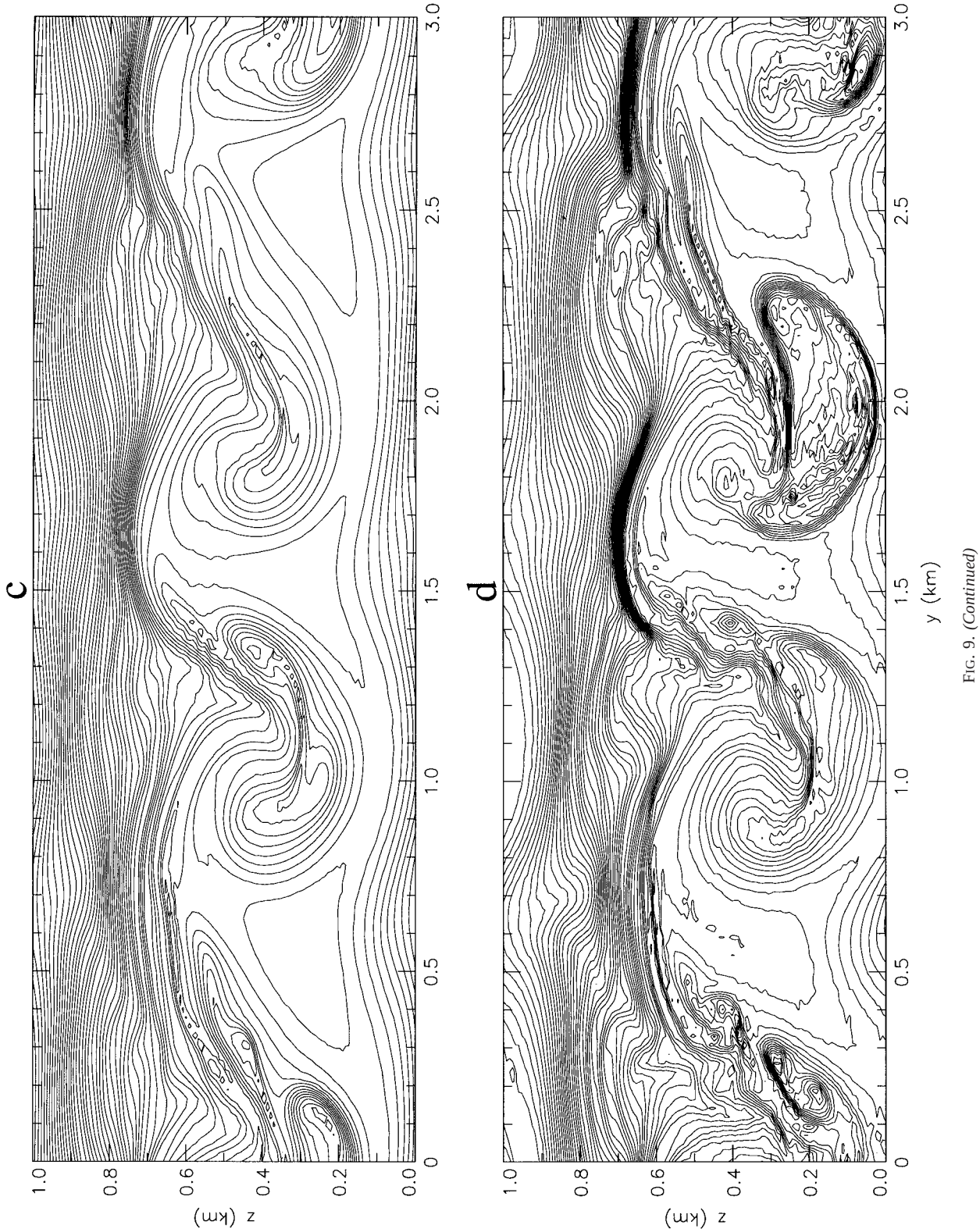

FIG. 9. *(Continued)*

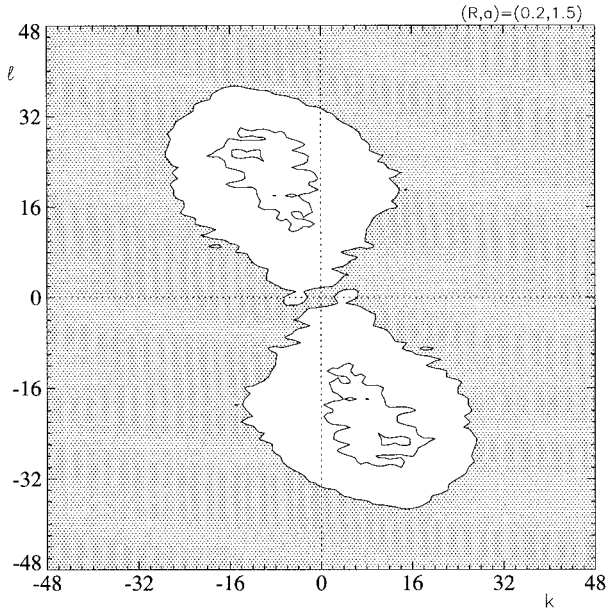

FIG. 10. Vertically integrated kinetic energy spectrum as in Fig. 1 but for $(R, a) = (0.2, 1.5)$.

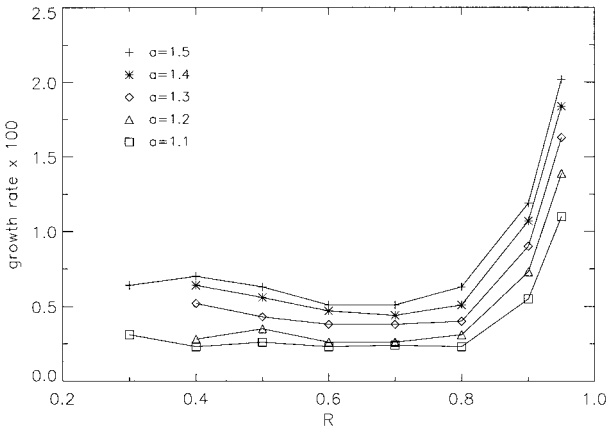

FIG. 11. Growth rates of most unstable modes as a function of R for convectively super-critical IGWs with $a = 1.1$–1.5.

physical space, the horizontal scale of instability is set approximately by the depth of the unstable shear layer, which is determined primarily by the value of λ_z, the vertical wavelength of the primary wave, and to a lesser extent by the wave amplitude a. Since λ_z and a are exactly constant in this sequence of runs, the horizontal wavelength of instability should not change appreciably. As it turns out, the horizontal scale is 1.4 km at $R = 0.95$ (corresponding to nondimensional wavenumber $\sim$21) and decreases slightly to 1.3 km at $R = 0.9$ and $R = 0.8$ (corresponding approximately to wavenumbers 16 and 10, respectively). The change of nondimensional wavenumber merely reflects the fact that λ_x, the horizontal wavelength of the primary wave, changes significantly between runs as implied by the IGW dispersion relation of LD1, Eq (2.4). [The primary wave has nondimensional wavenumber $(k, l) = (1, 0)$ in all cases.] Each of the three nondimensional wavenumbers then corresponds approximately to the same (dimensional) horizontal length in physical space.

b. Intermediate-frequency regime: 0.4 ≤ R ≤ 0.7

At $R = 0.7$, $a = 1.5$ a hint of a halo is visible at early times (not shown), but it does not persist. By the time the instability approaches finite amplitude, it is oriented primarily in the transverse direction as shown in Fig. 2a. The brief appearance of a halo spectrum, giving way to instabilities in the transverse (and possibly parallel) direction, are common features of the convectively supercritical, intermediate-frequency regime, which extends down to $R = 0.4$ (Figs. 2b–d). In each of the four cases shown, transverse or nearly transverse instabilities dominate up to the point of IGW breakdown.

To illustrate in detail the characteristics of transverse instability in the convectively unstable regime, we focus on a case similar to that of Fig. 2b at $R = 0.6$, but with smaller amplitude $a = 1.1$. The kinetic energy spectrum for this case is shown in Fig. 3. While the $R = 0.6$, $a = 1.5$ case in Fig. 2b displays qualitatively the same behavior as at $a = 1.1$, the transverse spectral peak is not as sharp. For this reason (and to demonstrate the markedly different behavior when the convective threshold is exceeded), we focus on the $a = 1.1$ case. In contrast to the convectively stable case at the same frequency discussed at length in LD1, the convectively unstable case does not exhibit any diagonal mode of instability. Instead, a localized peak at wavenumber 7 appears in the transverse direction, corresponding to a horizontal scale of about 1.1 km. This situation is essentially that of Fig. 2b, but in the latter case (with $a = 1.5$) the most unstable transverse wavenumber is smaller ($\sim$4)—presumably because the depth of the unstable shear layer increases slowly as a is increased and the horizontal scale is proportional to layer depth.

The development of transverse instability is illustrated in Figs. 4a–d at times when the perturbations attain finite amplitude and become visible in the total density field. Each figure panel is oriented in the transverse direction and located at the same value of x, showing the downward phase progression of the primary IGW. There are seven very similar cells that develop in the region of reduced static stability (indicated by the weak vertical density gradient). A vertical cross section of the x component of perturbation vorticity field reveals like-signed vortices reminiscent of Kelvin–Helmholtz billows (Fig. 5). The ''shear'' nature of instability is also confirmed by a plot of the vertical velocity perturbation shown in Fig. 6. The phase of the instability is tilted against the shear, implying a flow of energy from the mean shear to the instability. The vertical ve-

locity exhibits a single-lobe structure much like the one found by Dunkerton (1997) at $R = 0.6$, $a = 1.5$.

Animation of this sequence and others in various planes demonstrates that the transverse instabilities are not located at the exact center of the overturned region, but are displaced slightly above, presumably as a result of upward advection by the primary wave's vertical velocity.

The transverse instability is fully developed by the time a weaker parallel shear instability manifests itself as small ripples at the position of maximum vertical shear (Fig. 7). In this case, the vertical shear in the transverse component of IGW horizontal velocity has suppressed convection and is responsible for the scale selection of shear instability in that direction. In the parallel direction vertical shear also inhibits convection, but shear instability in that plane grows at a much slower rate than transverse instability. This picture is consistent with linear stability calculations, which predict the dominance of a transverse mode of shear instability and a weaker parallel shear instability at larger horizontal scales in this range of R (Dunkerton 1997).

Comparing this case to that of LD1, the behavior of shear instability at intermediate R is evidently quite sensitive to amplitude in the vicinity of the convective threshold $a = 1$. At slightly subcritical amplitudes, the timescale of instability is long compared to the timescale of the primary wave. The (asymptotically) dominant instability is one with apparent group velocity matching the horizontal phase velocity of the primary wave, as demonstrated in the Hovmöller diagram of LD1. At slightly supercritical amplitudes, the instability evolves on a faster timescale; thus, the assumptions of locally parallel, steady flow are better satisfied. The transverse mode predicted by linear stability theory emerges in place of the slower-growing diagonal mode.

We note incidentally that the diagonal mode appears at higher wave frequencies just above the convective threshold (not shown). However, it did not reach finite amplitude in any of the cases examined.

c. Higher-frequency regime: $0.2 \leq R \leq 0.3$, $a = 1.5$

At higher frequencies, the strength of the transverse vertical shear, and hence its ability to suppress convection in that plane, decreases. At $R = 0.3$, the spectrum still exhibits a sharp peak in the transverse direction at nondimensional wavenumber 4 (Fig. 8). The horizontal scale of instability has shrunk, relative to its value at lower frequencies, by nearly one-half (noting that nondimensional wavenumber 4 at $R = 0.3$ corresponds to a physical scale of 0.74 km). Density cross sections reveal the formation of coherent structures (Figs. 9a–d). However, unlike the tilted Kelvin–Helmholtz billows observed at $R = 0.6$, these structures appear to be more symmetric and do not roll up to the same degree as observed for shear instabilities in our lower-frequency runs. Animations of the density field suggest, rather, that the roll-up is arrested by vigorous three-dimensional convective events as depicted in Fig. 9d. These events resemble ''mushrooms'' or plume structures at late times. The presence of counterrotating vortices in the vorticity field (not shown) confirms the convective nature of these structures. Mean shear renders the convective cells slightly asymmetric: for example, the negative vortex appears slightly stronger than its positive counterpart, as expected since the vorticity due to the wave vertical shear is negative in this region.

At $R = 0.2$, the IGW shear is too weak to inhibit convection or cause scale selection. The spectrum exhibits a broadly diffuse region (Fig. 10), the radial extent of which is apparently governed by the model's hyperdiffusion. This is clearly indicative of broadband transverse convection, which was also observed in three-dimensional simulations of high-frequency (nonrotating) wave breakdown (Andreassen et al. 1994; Fritts et al. 1994; Isler et al. 1994; Fritts et al. 1996).

d. Instability growth rates

Figure 11 displays the estimated growth rate of most unstable modes as a function of R for waves of amplitude $a = 1.5$. Low-frequency waves experience the fastest growth rates of shear instability. Growth rates exhibit a minimum at about $R = 0.8$. To the left of this minimum, growth rates increase again; the influence of shear is becoming weaker. By $R = 0.2$, the instability can be classified as primarily convective. These results agree qualitatively with Dunkerton's (1997) stability analysis.

e. Summary

Figure 12 illustrates the various instability regimes encountered in this paper and in LD1 for convectively stable waves. The dominant asymptotic disturbances may be categorized as approximately isotropic shear instability at large R (H for halo, S for shear), diagonal shear instability at intermediate R and convectively stable a (DS), transverse shear instability at intermediate R and convectively unstable a (TS) modified by convection at slightly lower R (TS/C), and transverse convection at lowest R (TC).

4. Conclusions

The three-dimensional breakdown of a large-amplitude, convectively unstable inertia–gravity wave was examined numerically as a function of primary-wave frequency and amplitude. The results confirm that near-inertial waves break down preferentially via shear instability even when the primary wave is initially overturned, as anticipated by Dunkerton (1997). As in the convectively stable near-inertial regime, the spectrum of instability energy is approximately isotropic in azimuthal orientation. At intermediate frequencies, wave

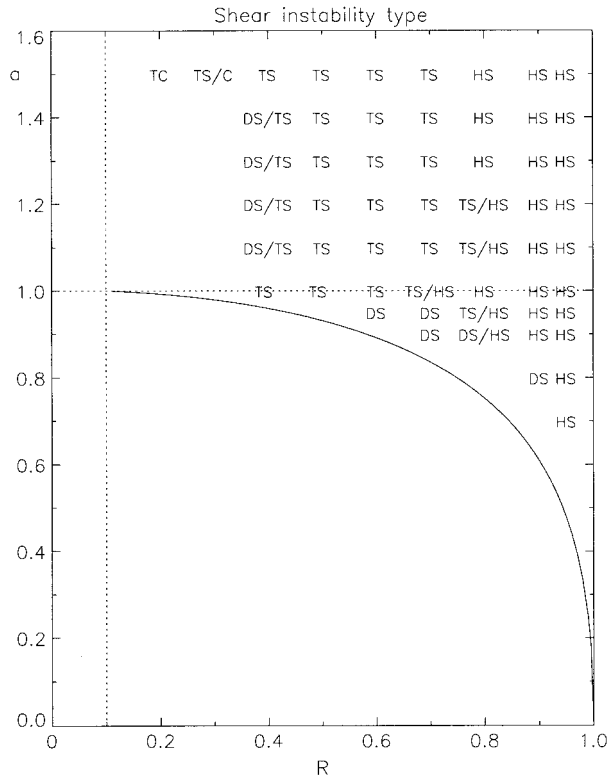

FIG. 12. Regime diagram for instabilities of convective stable and unstable IGW. The dominant asymptotic disturbances may be categorized as approximately isotropic shear instability at large R (H for halo, S for shear), diagonal shear instability at intermediate R and convectively stable a (DS), transverse shear instability at intermediate R and convectively unstable a (TS) modified by convection at slightly lower R (TS/C), and transverse convection at lowest R (TC).

breakdown is triggered by a transverse shear instability in the region of overturning. This behavior, displaying a clear preference for instability with horizontal component of wave vector in the transverse direction, is different from the breakdown of convectively stable waves at intermediate frequency examined in Part I, in which diagonal modes were preferred. As the primary wave frequency is increased further, shear instabilities once again develop in the transverse direction, but are modified by convective instability as the billows reach finite amplitude. The influence of transverse vertical shear becomes progressively weaker as the wave frequency approaches the buoyancy frequency. In this limit, transverse convection leads to wave collapse, and there is no preferred scale of instability.

In Parts I and II of this series, we have identified the principal modal instabilities that lead to IGW breakdown in the range $0.2 \leq R \leq 0.95$ with $N/f = 10$. Certain issues, however, remain unresolved and need to be addressed. In LD1, we showed that the behavior of the instability for low-frequency IGWs does not change appreciably as N/f is increased. At higher frequencies, the functional dependence on N/f is less clear. From the limited number of runs performed up to now at higher values of N/f, there is some indication that the properties of the diagonal shear mode depend upon this parameter. Insofar as the diagonal mode was not anticipated by theoretical analysis based on a steady, parallel-flow approximation at real horizontal wavenumber (Dunkerton 1997), but appears in a Floquet analysis (Klassen and Yan 1996, personal communication), further theoretical and numerical study of the dynamics of this mode is warranted. Also, the direct effect of rotation on unstable perturbations must be considered when N/f is artificially reduced.

An interesting aspect of the problem, not touched upon here, is the temporal evolution of the locus of unstable modes. At low frequencies, the halo structure emerges rapidly and does not evolve significantly over time. The behavior becomes more complicated at the higher frequencies, especially in the transitional regions of parameter space. For example, at $R = 0.8$, we noted that over the course of the linear growth phase, the instabilities may exhibit in turn the characteristics of HS, TS, and DS (using the notation of section 3e). Our focus in this study has been primarily on modal instabilities, yet early-time growth due to nonmodal structures may be significant as well. Modal instabilities represent asymptotic behavior at infinite time starting from vanishingly small initial amplitude; as such, they represent a special case of instability, which, in general, occurs in a finite time beginning from a noise spectrum of finite amplitude. The instability of large-amplitude IGWs in a realistic background spectrum should be investigated if these results are to be related to actual situations in the atmosphere and ocean.

IGWs typically encounter regions of changing static stability or mean wind as they propagate vertically. One way to render our problem more realistic is to allow for the amplitude to evolve, using an artificial forcing term, to simulate the propagation of an IGW in a variable basic state. This approach would, among other things, enable us to assess the likelihood or otherwise of IGWs ''saturation'' via dynamical shear instability, and the relevance of supercritical wave amplitudes as a function of R.

Acknowledgments. This research was supported by the National Science Foundation, Grants ATM-9123797, ATM-9500613, and OCE-9521275, and by the Air Force Office of Scientific Research, Contract F49620-92-C-0033. The computations were performed on the Cray C90 at the Pittsburgh Supercomputing Center and on the Cray Y-MP and Cray J916 at the National Center for Atmospheric Research. Discussions with Donal O'Sullivan, Jim Riley, and Pete Lombard during the course of this work are gratefully acknowledged.

REFERENCES

Andreassen, O., C. E. Wasberg, D. C. Fritts, and J. R. Isler, 1994: Gravity wave breaking in two and three dimensions. Part I: Mod-

el description and comparison of two-dimensional evolutions. *J. Geophys. Res.,* **99,** 8095–8108.

Deardorff, J. W., 1965: Gravitational instability between horizontal plates with shear. *Phys. Fluids,* **8,** 1027–1030.

Dunkerton, T. J., 1984: Inertia-gravity waves in the stratosphere. *J. Atmos. Sci.,* **41,** 3396–3404.

——, 1997: Shear instability of internal inertia-gravity waves. *J. Atmos. Sci.,* **54,** 1628–1641.

——, and R. E. Robins, 1992: Radiating and nonradiating modes of secondary instability in a gravity-wave critical layer. *J. Atmos. Sci.,* **49,** 2546–2559.

Fritts, D. C., and P. K. Rastogi, 1985: Convective and dynamical instabilities due to gravity wave motions in the lower and middle atmosphere: Theory and observations. *Radio Sci.,* **20,** 1247–1277.

——, and L. Yuan, 1989: Stability analysis of inertio-gravity wave structure in the middle atmosphere. *J. Atmos. Sci.,* **46,** 1738–1745.

——, J. R. Isler, and O. Andreassen, 1994: Gravity wave breaking in two and three dimensions. Part II: Three dimensional evolution and instability structure. *J. Geophys. Res.,* **99,** 8109–8123.

——, J. F. Garten, and O. Andreassen, 1996: Wave breaking and transition to turbulence in stratified shear flows. *J. Atmos. Sci.,* **53,** 1057–1085.

Hazel, P., 1972: Numerical studies of the stability of inviscid stratified shear flows. *J. Fluid Mech.,* **51,** 39–61.

Isler, J. R., D. C. Fritts, O. Andreassen, and C. E. Wasberg, 1994: Gravity wave breaking in two and three dimensions. Part III: Vortex breakdown and transition to isotropy. *J. Geophys. Res.,* **99,** 8125–8137.

Lelong, M.-P., and T. J. Dunkerton, 1998: Inertia-gravity wave breaking in three dimensions. Part I: Convectively stable waves. *J. Atmos. Sci.,* **55,** 2473–2488.

Lombard, P. N., and J. J. Riley, 1996: On the breakdown into turbulence of propagating internal waves. *Dyn. Atmos. Oceans,* **23,** 345–355.

Walterscheid, R. L., and G. Schubert, 1990: Nonlinear evolution of an upward propagating gravity wave: Overturning, convection, transience and turbulence. *J. Atmos. Sci.,* **47,** 101–125.

Winters, K. B., and E. A. D'Asaro, 1989: Two-dimensional instability of finite amplitude internal gravity wave packets near a critical level. *J. Geophys. Res.,* **94,** 12 709–12 719.

——, and J. J. Riley, 1992: Instability of internal waves near a critical layer. *Dyn. Atmos. Oceans,* **16,** 249–278.

——, and E. A. D'Asaro, 1994: Three-dimensional wave instability near a critical level. *J. Fluid Mech.,* **272,** 255–284.